LETTERS

Slip on 'weak' faults by the rotation of regional stress in the fracture damage zone

D. R. Faulkner[1], T. M. Mitchell[1], D. Healy[1]† & M. J. Heap[1]†

Slip on unfavourably oriented faults with respect to a remotely applied stress is well documented and implies that faults such as the San Andreas fault[1] and low-angle normal faults[2] are weak when compared to laboratory-measured frictional strength[3]. If high pore pressure within fault zones is the cause of such weakness, then stress reorientation within or close to a fault is necessary to allow sufficient fault weakening without the occurrence of hydrofracture[4]. From field observations of a major tectonic fault, and using laboratory experiments and numerical modelling, here we show that stress rotation occurs within the fractured damage zone surrounding faults. In particular, we find that stress rotation is considerable for unfavourably oriented 'weak' faults. In the 'weak' fault case, the damage-induced change in elastic properties provides the necessary stress rotation to allow high pore pressure faulting without inducing hydrofracture.

The concept of stress rotation within fault zones is important to understand the strength of fault zones that are unfavourably oriented with respect to the remotely applied driving stress ('weak' faults). The San Andreas 'stress–heat flow paradox' (where slip is implied at low shear stresses)[1,5] and slip on low-angle normal faults[2,6] imply that fault weakening occurs. Possible explanations include weak fault materials[7], dynamic slip weakening[8,9] and elevated pore fluid pressures[4,10,11]. Stress rotation within the fault zone (as a consequence of mean stress increase, differential stress decrease and mechanical continuity) must accompany high pore fluid pressures, or effective σ_3 will be pushed well into the tensile field. This would result in hydrofracture, pore fluid pressure loss and fault strengthening[4]. Stress rotations around faults have been inferred from seismological studies[12,13]. Previously, stress rotation has been postulated to occur in the narrow fault gouge core either by Coulomb plasticity[14] or by material softening[4]. One consequence of invoking stress rotation within a deforming narrow ductile fault gouge layer is that a limiting condition occurs where σ_1 is oriented at 45° to the fault plane at the boundary of the gouge layer[4,14]. Some workers have suggested that this soft gouge layer would be subject to extrusion as the deformation progresses[15].

Faults consist of a single or multiple core zone where rock flour (gouge) accommodates the vast majority of strain, surrounded by a fractured 'damage' zone[16,17]. We measure the density of the microfractures in the damage zone of a major strike–slip fault, and relate these to elastic property changes measured in laboratory experiments. Stress modelling shows that significant changes in the stress field occur within the fault damage zone.

We have studied the damage zone surrounding the Caleta Coloso fault, a >5-km-offset strike-slip fault in the Atacama fault system of northern Chile[18]. The fault cuts through crystalline rocks of predominantly granodioritic composition. The fault was exhumed and currently displays fault zone structures formed at depths of 4–10 km that are particularly well exposed and preserved owing to the hyperarid climate. We collected samples at regular intervals within the fracture damage zone as a function of distance from the fault core for microstructural analysis. Microfracture densities were measured (represented by fluid inclusion planes—see Fig. 1) in quartz grains within the samples. Although the microfractures within the samples are healed (fluid inclusion planes), they are likely to have remained open for significant periods of the fault's history. Hydrothermal cementation of fractures in the region shows only minor disturbance by later fault movements, supporting this inference. Open fractures in the damage zone are expected during fault movement when the fault is more or less critically stressed, as shown by well-connected fluid pathways that keep fluid pressures hydrostatic in intraplate

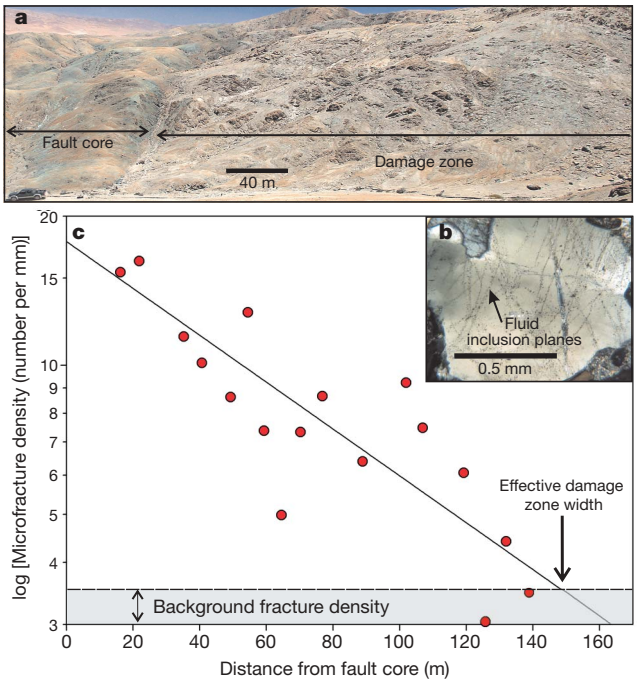

Figure 1 | Field data showing the variation in microfracture density within the fault damage zone. a, View looking south along the strike of the Caleta Coloso fault, showing the fault core zone to the left and fault damage zone from which samples were taken for analysis on the right. **b**, Example of quartz grain containing fluid inclusion planes. **c**, Microfracture (fluid inclusion plane) density versus distance from the fault core. The line indicates a least-squares fit to the data. Background fracture density is shown for reference.

[1]Rock Deformation Laboratory, Department of Earth and Ocean Sciences, University of Liverpool, Liverpool, L69 3GP, UK. †Present addresses: Department of Earth Sciences, University of Durham, Durham, DH1 3LE, UK (D.H.); Mineral, Ice and Rock Physics Laboratory, Department of Earth Sciences, University College London, Gower Street, London, WC1E 6BT UK (M.J.H.).

regions[19]. This damage-zone permeability contrasts with the low permeability of fault cores capable of maintaining fluid overpressure[11].

Quartz was selected for microfracture analysis because it has little fracture anisotropy and hence is a good proxy for the total amount of damage the rock has sustained. Figure 1 shows that microfracture density falls exponentially with distance from the fault core, and is in accordance with other observations of microfracture damage surrounding lower displacement faults[20,21]. Our microfracture densities are lower than in previous studies, perhaps owing to the smaller proportion of quartz and fracturing within feldspars. However, we suggest that the data are representative of the relative amount of microfracture damage that the rock has sustained. Having established the distribution of microfractures surrounding faults, we now consider the role of microfracturing on the elastic properties of crystalline rock from laboratory experiments.

We performed uniaxial cyclic loading, increasing stress amplitude tests on 25.4-mm-diameter cores of Westerly granite. Westerly granite was chosen for experiments in preference to the granodiorite because of fine grain size and low initial microfracture density. However, because both are low-porosity, crystalline rocks, Westerly granite should provide a representative data set that can be related to granodiorite. Details of the experiments are given in the Methods section.

Multiple tests were conducted with different numbers of increasing amplitude stress cycles so that the samples could be thin-sectioned to establish the density of microfractures as a function of number of cycles. The peak stress for the first cycle was 80 MPa and it was increased by 12 MPa in each subsequent cycle. The elastic parameters were measured in the final unloading–loading stress cycle before thin sectioning. The results are shown in Fig. 2. We chose a differential stress value of 60 MPa to observe the change in the elastic parameters resulting from damage due to the increasing number of cycles. This value is ~30% of the failure stress of the rock. If the rock underwent failure in nature, microfractures would form at or near the peak stress immediately before fault formation, whereupon the stress would drop to that required for frictional sliding. Microfractures may also occur as a product of irregularities on the fault, or from dynamic loading[22,23]. Figure 2 shows a reduction in Young's modulus of ~6.5 GPa, and an increase in Poisson's ratio of ~0.2 related to increasing microfracture density as the sample approached failure.

Despite having collected our data in the absence of confining pressure, which might serve to suppress the formation of new microfractures, we believe that the changes in the elastic parameters are representative of those at depth. Although we are not aware of any tests that have been performed to establish the static elastic parameters under confining pressure, we have compared our results to tests where dynamic elastic parameters were obtained from ultrasonic wave velocities measured during progressive fracture[24]. The magnitudes of the change of these properties ($\Delta E \approx 10$ GPa) compare favourably to our results. Our tests were also conducted under atmospheric conditions and so we have not established the effects of water saturation and elevated fluid pressure on the results.

Thus far we have shown that microfracture density varies as a function of distance from faults and that increasing microfracture damage strongly affects the elastic properties of rocks. We now combine these data to predict the effect these changes have on a remotely applied stress field in the vicinity of a fault.

We developed a two-dimensional plane-strain model to calculate the stress field in a horizontal plane cutting a vertical strike–slip fault zone. The model differs from that of Rice[4] in that we do not assume a rigid–plastic rheology with an actively deforming Von Mises plastic layer, but rather a statically loaded fault system with several layers of material having elastic properties that vary systematically with distance from the fault core. We justify this static case by relating it to either a locked fault in the interseismic period, or a creeping fault, where the stresses within the damage zone would be at a more or less constant level. The model is similar to that of Casey[25] but we represent the damage zone as a series of discrete fault-parallel layers, each with a specific Young's modulus and Poisson's ratio.

Because the laboratory experiments were performed on Westerly granite and the microfracture densities in the field were measured in

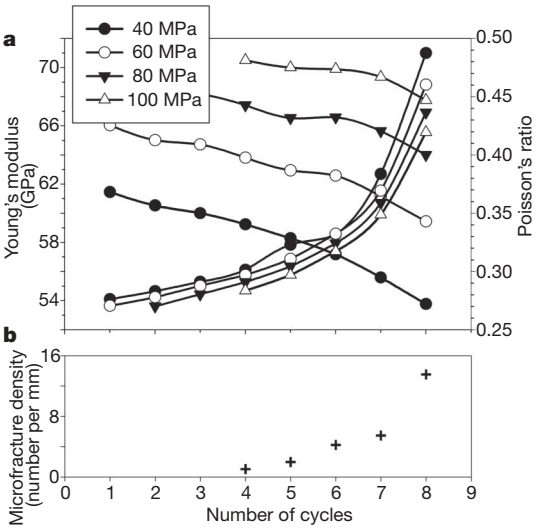

Figure 2 | Variation of measured elastic properties with increasing microfracture damage in Westerly granite. **a**, Change in Young's modulus (increasing curves) and Poisson's ratio (decreasing curves) with increasing damage. Data are shown for stresses of 40, 60, 80 and 100 MPa. Cycle 1 was taken to a maximum stress of 80 MPa and the stress was increased by ~12 MPa on each subsequent cycle. **b**, Increase in microfracture density with increasing damage.

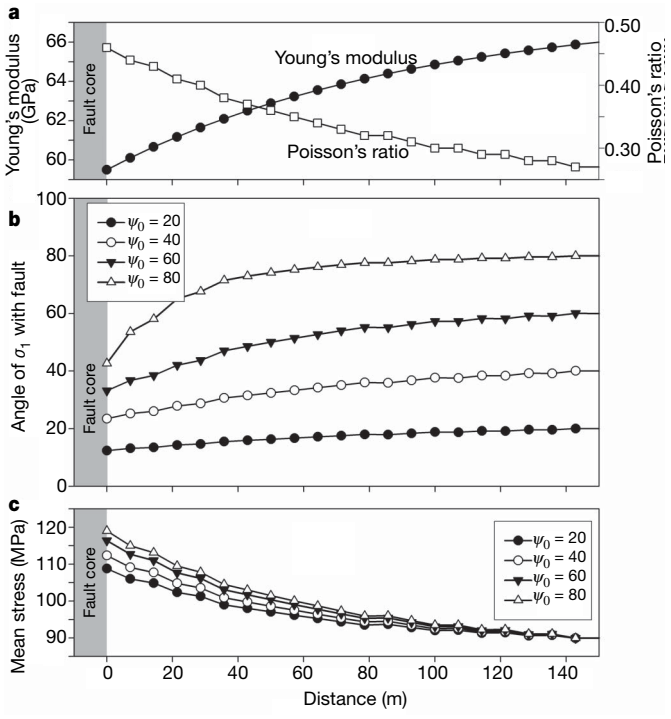

Figure 3 | Variation of elastic properties, principal stress orientation and the mean stress as a function of distance within the fault damage zone. **a**, Values for elastic properties versus distance from the fault core used for the modelling. **b**, Change in angle ψ between the fault plane and the maximum compressive stress σ_1 with distance from the fault core. ψ_0 is the value of ψ outside the damage zone. **c**, Change in the mean stress with distance from the fault core.

granodiorite, we relate the two sets of microfracture densities by assuming that the elastic properties of the Westerly granite after one stress cycle represent those of the granodiorite at the edge of the fracture damage zone, and that the elastic properties of the granite closest to failure represent those of the granodiorite adjacent to the fault core. The elastic property data are scaled according to the microfracture density. Figure 3a shows how the elastic parameters vary as a function of distance from the fault core. In cartesian coordinates, with x parallel to the fault and y normal to the fault, we imposed the following boundary conditions for stress σ and strain ε for cohesive (no slip) contacts between each layer n:

$$(\sigma_{yy})_n = (\sigma_{yy})_{n+1}$$

$$(\tau_{yx})_n = (\tau_{yx})_{n+1}$$

$$(\varepsilon_{xx})_n = (\varepsilon_{xx})_{n+1}$$

Assuming mechanical equilibrium, the equations relating normal and shear stress and strain for each layer could then be solved in the same way as in ref. 25. The calculated cartesian stress components were then converted into principal stresses using the appropriate transformation equations[26].

We selected remotely applied principal stress values of 120 and 60 MPa. Using these values gives a differential stress of 60 MPa: the same differential stress at which we measured our elastic parameters in the laboratory. The model results are shown in Fig. 3b and c. A remotely applied σ_1 oriented at 80° to the fault plane will rotate in the damage zone such that the fault core will only 'see' local stresses that are oriented at an angle of 42° to the fault plane. The amount of rotation is less for smaller angles between σ_1 and the fault plane. The mean stress, as well as the values of σ_1 and σ_3, increases as the fault core is approached, with an overall decrease in the differential stress (Figs 3c and 4). The Poisson's ratio has a larger effect on the rotation of stress than the Young's modulus. These trends have been predicted previously[4] for stress rotations within a 'weak' gouge layer but only in a qualitative way. In our model, the stress imposed on the fault core has already been rotated throughout the damage zone, and we have quantified the magnitude of the stress rotation and modification of the principal stresses using field and laboratory data.

The results from our model are applicable to all brittle faults formed within low-porosity rocks where microfracture damage and dilatancy accumulate during deformation. If a fault zone has an associated fracture damage zone, then stresses will be modified and rotated according to the change in elastic properties of the damaged material. Faults running through lithologies different from that described here might undergo different quantities of stress modification, but the trend should be equivalent. In Fig. 3, we have placed a scale on the abscissa to relate our data specifically to its distance from the Caleta Coloso fault core. However, our model is scale invariant and so lower displacement faults, perhaps with smaller damage zones, should still undergo similar stress modification if the elastic property changes are commensurate with those we measured. The type of fault zone, either with a single[16] or multiple core[17] should not affect the surrounding damage zone. With regard to fault gouge extrusion[15], we note that the fault core in large faults is only a small proportion of the width of the fault zone[16,17]. Hence only minor extrusion would be possible before asperities would contact, and because our model does not rely on stress modification in the gouge zone, stress changes within the damage zone would still allow pore pressure weakening without hydrofracture.

In this paper we consider only the effect of microfractures on the bulk elastic properties of the rock. In fault damage zones, macroscopic fractures are present but their effect is on too large a scale for laboratory measurements and hence are not discussed here. However, the presence of macrofractures will further affect the bulk elastic properties and hence our analysis could be thought of as the minimum effect that might be seen.

We emphasize that although stresses are rotated to favourable angles, stress rotation alone does not bring an unfavourably oriented fault closer to failure[4,25]. One of our model boundary conditions is that the normal and shear stresses between each fault-parallel layer are equal. Figure 4 shows the modification of the stress field in the fracture damage zone, and the fixed normal and shear stresses resolved parallel to the fault plane. For failure to occur, fault zone weakening is still required, but stress rotation within the damage zone allows high pore fluid pressure to develop without hydrofracture and rupture of any hydraulic seal present. Our model is quantitatively based on field and laboratory measurements and circumvents the problems associated with invoking stress rotation within the narrow gouge layer of the fault core.

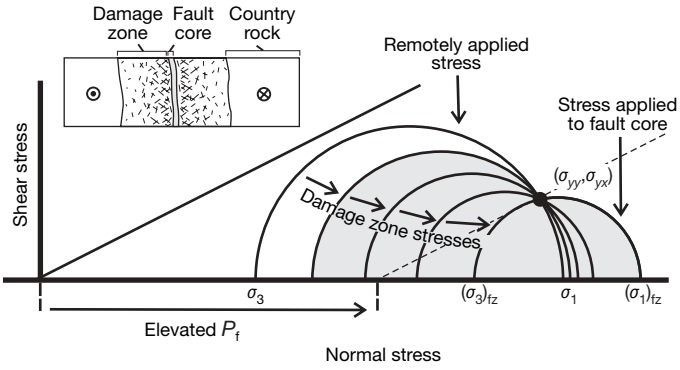

Figure 4 | Mohr diagram illustrating the stress rotation within the damage zone. Schematic Mohr diagram showing the change in the state of stress within the damage zone (shaded circles) to the fault core (fz). The two failure envelopes show the case of an unpressurized fault core (solid line) and pressurized fault core (dashed line), where P_f denotes the pore fluid pressure. Note that the normal stress and shear stress resolved on the fault plane are fixed and do not change from the remotely applied stress to the fault plane. The inset shows a schematic diagram of fault zone structure illustrating the core zone, damage zone and country rock.

METHODS

In the experiments, the axial and circumferential strain were both measured as a function of stress during loading and unloading and from these data the elastic parameters, Young's modulus E and Poisson's ratio ν, were calculated. The stress–strain curves look like typical uniaxial stress–strain curves, but with multiple cycles. Unlike previous uniaxial compression tests that have been used to determine the static elastic properties of rocks, we have extended the range of stress values for which values of the elastic properties can be obtained. In the post-yield phase of loading, the loading–unloading curves display hysteresis. We worked around this by fitting third-order polynomial functions (to capture the true form of the stress–strain curve) to the loading and unloading stress strain curves that can then be differentiated to obtain the gradient. The gradients of an unloading curve were then compared with the gradients for the next loading curve (to ensure the rock did not incur any further microfracture damage between the two curves until the previous highest stress in the unloading curve was exceeded), and the range of stress values for which the gradients were the same were then used to calculate the elastic parameters[27]. In this way, elastic constants were obtained over a wide range of stress values.

Our data show that the Poisson's ratio does not extend above 0.5—an indication of the validity of our approach. Our approach means that the elastic parameters immediately before failure are not recorded and are likely to have a greater range than those measured, and hence the data we use for modelling may be seen as conservative, lower-bound values for the elastic properties. Thus the effects described later are a minimum response of the stress orientation and magnitude.

Received 25 May; accepted 12 October 2006.

1. Zoback, M. D. *et al.* New evidence on the state of stress of the San Andreas fault system. *Science* **238**, 1105–1111 (1987).

2. Colletini, C. & Sibson, R. H. Normal faults, normal friction? *Geology* **29,** 927–930 (2001).
3. Byerlee, J. D. Friction of rocks. *Pure Appl. Geophys.* **116,** 615–629 (1978).
4. Rice, J. R. in *Fault Mechanics and Transport Properties of Rocks* (eds Evans, B. & Wong, T.-f.) 475–503 (Academic Press, San Diego, CA, 1992).
5. Lachenbruch, A. H. & Sass, J. H. Heat flow and energetics of the San Andreas fault zone. *J. Geophys. Res.* **85,** 6185–6223 (1980).
6. Sibson, R. H. An assessment of field evidence for ''Byerlee'' friction. *Pure Appl. Geophys.* **142,** 645–662 (1993).
7. Morrow, C. A., Moore, D. E. & Lockner, D. A. The effect of mineral bond strength and absorbed water on fault gouge frictional strength. *Geophys. Res. Lett.* **27,** 815–819 (2000).
8. Wibberley, C. A. J. & Shimamoto, T. Earthquake slip weakening and asperities explained by thermal pressurization. *Nature* **436,** 689–692 (2005).
9. Di Toro, G., Hirose, T., Nielsen, S., Pennacchioni, G. & Shimamoto, T. Natural and experimental evidence of melt lubrication of faults during earthquakes. *Science* **311,** 647–650 (2006).
10. Byerlee, J. D. Friction, overpressure and fault-normal compression. *Geophys. Res. Lett.* **17,** 2109–2112 (1990).
11. Faulkner, D. R. & Rutter, E. H. Can the maintenance of overpressured fluids in large strike-slip fault zones explain their apparent weakness? *Geology* **29,** 503–506 (2001).
12. Hardebeck, J. L. & Hauksson, E. Role of fluids in faulting inferred from stress field signatures. *Science* **285,** 236–239 (1999).
13. Provost, A-S. & Houston, H. Orientation of the stress field surrounding the creeping section of the San Andreas fault: Evidence for a narrow mechanically weak fault zone. *J. Geophys. Res.* **106,** 11373–11386 (2001).
14. Lockner, D. A. & Byerlee, J. D. How geometrical constraints contribute to the weakness of mature faults. *Nature* **363,** 250–252 (1993).
15. Scholz, C. H. Evidence for a strong San Andreas fault. *Geology* **28,** 163–166 (2000).
16. Chester, F. M., Evans, J. P. & Biegel, R. L. Internal structure and weakening mechanisms of the San Andreas fault. *J. Geophys. Res.* **98,** 771–786 (1993).
17. Faulkner, D. R., Lewis, A. C. & Rutter, E. H. On the internal structure and mechanics of large strike-slip faults: field observations from the Carboneras fault, southeastern Spain. *Tectonophysics* **367,** 235–251 (2003).
18. Cembrano, J. *et al.* Fault zone development and strain partitioning in an extensional strike-slip duplex: a case study from the Atacama Fault System, northern Chile. *Tectonophysics* **400,** 105–125 (2005).
19. Townend, J. & Zoback, M. D. How faulting keeps the crust strong. *Geology* **28,** 399–402 (2000).
20. Vermilye, J. & Scholz, C. H. The process zone; a microstructural view of fault growth. *J. Geophys. Res.* **103,** 12223–12237 (1998).
21. Anders, M. H. & Wiltschko, D. V. Microfracturing, paleostress and the growth of faults. *J. Struct. Geol.* **16,** 795–815 (1994).
22. Wilson, J. E., Chester, J. S. & Chester, F. M. Microfracture analysis of fault growth and wear processes, Punchbowl Fault, San Andreas system, California. *J. Struct. Geol.* **25,** 1855–1873 (2003).
23. Rice, J. R., Sammis, C. G. & Parsons, R. Off-fault secondary failure induced by a dynamic slip pulse. *Bull. Seismol. Soc. Am.* **95,** 109–134 (2005).
24. Ayling, M. R., Meredith, P. G. & Murrell, S. A. F. Microcracking during triaxial deformation of porous rocks monitored by changes in rock physical properties. I. Elastic-wave propagation measurements on dry rocks. *Tectonophysics* **245,** 205–221 (1995).
25. Casey, M. Mechanics of shear zones in isotropic dilatant materials. *J. Struct. Geol.* **2,** 143–147 (1980).
26. Jaeger, J. C. & Cook, N. G. W. *Fundamentals of Rock Mechanics* 11–17 (Chapman and Hall, London, 1976).
27. Heap, M. J. & Faulkner, D. R. Quantifying the evolution of static elastic properties as crystalline rock approaches failure. *J. Struct. Geol.* (submitted)

Acknowledgements We thank J. Cembrano for field assistance and M. Casey, N. Kusznir and D. Prior for discussions. This work was supported by the Natural Environment Research Council and the Nuffield Foundation.

Author Information Reprints and permissions information is available at www.nature.com/reprints. The authors declare no competing financial interests. Correspondence and requests for materials should be addressed to D.R.F. (faulkner@liv.ac.uk).